Semaglutide interferes with postnatal growth in a diet-dependent manner

Amélie Joly[1]*, Lucas Rebiffé[1]*, Yves Dusabyinema[1], Julien Dellinger[1], François Leulier[1] & Filipe De Vadder[1 †]

[1] Institut de Génomique Fonctionnelle de Lyon, École Normale Supérieure de Lyon, CNRS UMR 5242, UCBL Lyon-1, F-69007 Lyon, France

* These authors contributed equally to this work

[†] To whom correspondence should be addressed: filipe.de_vadder@ens-lyon.fr

Highlights (3 to 5, 85 characters max per point):

- Semaglutide hampers the growth of protein-malnourished, but not control-fed, juvenile animals.
- The effects of semaglutide on linear growth are independent of alterations in the somatotropic axis.
- Semaglutide differentially alters glucose metabolism of juvenile mice depending on their dietary protein intake.

Abstract:

Objective

Glucagon-like peptide 1 receptor agonists (GLP-1RAs) have been shown to impact glucose homeostasis and, more recently, the somatotropic axis. While the effects of GLP-1RAs have been extensively studied in the context of diet-induced obesity, their impact on physiology in other nutritional contexts have been less explored. We investigated the potential beneficial effects of the GLP-1RA semaglutide during juvenile protein malnutrition, a dietary challenge known to cause stunted growth and to disrupt metabolic homeostasis.

Methods

We used a murine model to assess the effects of twice-weekly subcutaneous injections of semaglutide during juvenile protein malnutrition. Glucose metabolism was evaluated through *in vivo* oral glucose tolerance test, *ex vivo* glucose-stimulated insulin secretion in isolated pancreatic islets and histology of the pancreas. We combined linear growth monitoring, analysis of the growth hormone/insulin-like growth factor 1 signaling pathway and liver bulk RNA sequencing to characterize the effects of semaglutide on the somatotropic axis during juvenile protein malnutrition.

Results

Semaglutide improved glucose tolerance in control and malnourished mice, but differentially impacted pancreatic islet physiology depending on the dietary protein intake. While semaglutide did not alter growth in control conditions, it further inhibited growth of malnourished mice associated with reduction in fat but not lean mass. Surprisingly, semaglutide had no discernible effect on the functionality of the somatotropic axis in malnourished mice. Liver transcriptomics revealed that semaglutide may interfere with the growth of malnourished juvenile mice by altering circadian rhythm and thermogenesis.

Conclusions

Our data reveal that semaglutide interacts differentially with the physiology of juvenile mice depending on their dietary protein intake. We found that semaglutide influences glucose metabolism and linear growth in a diet-dependent manner, underscoring the importance of examining the effects of GLP-1RAs across various nutritional contexts and developmental stages.

Keywords: Semaglutide, protein malnutrition, somatotropic axis, circadian rhythm

1. **Introduction**:

In recent years, GLP-1 receptor agonists (GLP-1RAs) have emerged as significant therapeutic options for managing type 2 diabetes and obesity. As of 2024, seven GLP-1RAs are approved by the US Food and Drug Administration for the treatment of type 2 diabetes [1]. Among them, semaglutide was optimized to have a longer half-life in humans and a better resistance to DPP-IV inhibitors than other GLP-1RAs [2]. Semaglutide improves glycemic control through pleiotropic mechanisms, including increased insulin secretion in response to glucose stimulation and improved beta cell survival and proliferation [3]. Besides its effects on glucose homeostasis, semaglutide also lowers energy intake and induces remarkable weight loss [1], [4]. Hence, it is now widely used to treat obesity in both adults [5], [6] and children [7].

In mammals, linear growth is regulated by the somatotropic axis, which is governed by growth hormone (GH) and insulin-like growth factor 1 (IGF-1). Interestingly, both *in vitro* and *in vivo* work on rodents demonstrated that GLP-1RAs can affect growth-related phenotypes by modulating osteoblast physiology [8], [9]. Besides, several studies in mice showed that GLP-1 and GLP-1RAs stimulate IGF-1 receptor (IGF-1R) expression [10], [11], favor bone metabolism homeostasis [8], [12] and even directly cross-activate the IGF-1R [13]. In addition, short- or long-term administration of GLP-1RAs in healthy adult volunteers could elicit an increase in circulating GH levels [14]. Thus, it has been recently suggested that, in addition to their effects

on energy homeostasis, GLP-1RAs, such as semaglutide, could interact with the GH/IGF-1 axis [15].

While the efficacy of semaglutide has been extensively studied in the context of diet-induced obesity, its effects upon other nutritional contexts where energy homeostasis is disrupted have received comparatively less attention. Notably, protein malnutrition during the juvenile period leads to intense alterations of the energy balance, including impairment of insulin production [16], [17] and overall worsening of glycemic control [18], [19]. In addition to disruption of energy homeostasis, chronically protein-malnourished children suffer from growth disturbances including stunting, defined as a low height-for-age [20]. Given the scarcity of human samples, murine models have been implemented in order to better understand the mechanisms underlying the physiological response to juvenile malnutrition. We and others have demonstrated that murine models of malnutrition recapitulate the alterations in growth and glucose metabolism observed in malnourished children [21], [22], [23].

Yet, the role of GLP-1RAs in modulating energy balance and growth during juvenile malnutrition, a period marked by significant disruptions in these processes, remain largely unexplored. Here, we aimed at examining the effects of the GLP-1RA semaglutide on glucose homeostasis and growth in a mouse model of juvenile protein malnutrition and to investigate the extent to which semaglutide could compensate for these phenotypes induced by protein malnutrition. We report that semaglutide differentially interacts with the glucose metabolism of juvenile mice depending on the diet and hampers the growth of malnourished, but not control, animals. Semaglutide-mediated effects on linear growth are independent of alterations of the somatotropic axis. In contrast, liver transcriptomic data indicate that semaglutide may interfere with the growth of malnourished juvenile mice by altering circadian rhythm and thermogenesis.

2. Material and methods:

2.1 Animals and treatments

All animal procedures have been approved by a local animal care and use committee (CECCAPP) and subsequently authorized by the French Ministry of Research (APAFIS #40481-2022103017295302 v3).

21-day-old C57BL/6N male mice were purchased from Charles River and weaned on AIN93G diet or on an isocaloric modified version of the AIN93G designed to be low in protein. Detailed composition of the diets is given in Table 1. Animals were weighted and measured weekly following a short isoflurane anesthesia. They received a subcutaneous injection of 30 nmol/kg body weight semaglutide (Ozempic, Novo Nordisk 0.5 mg injectable solution) or saline solution (thereafter NaCl or vehicle) twice a week until postnatal day 56 (P56). At P56, animals were fasted during 6 hours starting at 8 AM and killed by cervical dislocation at 2 PM.

Blood and organs were sampled. Left femur and tibia were dissected and precisely measured using a caliper.

For oral glucose tolerance test, mice were fasted during 6h and orally gavaged with a 20% D-(+)-glucose solution (Sigma Aldrich, G7021) at a dose of 1 g/kg body weight. Blood glucose levels were measured from the tail vein before (0 min) and at 15, 30, 60, 90, 120 min after glucose gavage using a hand-held glucometer (OneTouche Verio reflect). Blood serum samples were collected from the tail vein at 0, 15 and 30 min after gavage. Samples were kept at -20°C.

We decided to restrict our study to male mice because we have previously shown that juvenile malnourished males display a stronger phenotype than malnourished females [24].

2.2 Pancreatic islet metabolic phenotyping

Pancreatic islets were isolated as previously described [25]. Briefly, the pancreas was inflated through common bile duct Collagenase XI (Sigma Aldrich, C7657) injection, mechanically disrupted using scissors and gentle shaking, and incubated with collagenase for 15 min at 37°C. Single islets were then hand-picked, put in fresh medium (1X DMEM, ThermoFisher, 31885-023; 5% FBS, Sigma Aldrich, F7524) and incubated overnight at 37°C.

The glucose-stimulated insulin secretion (GSIS) assay was performed by following the static assay described by Zhu *et al.* in a 48 well-plate [26]. Briefly, 10 islets per well were equilibrated 1 h in DMEM containing 1 g/L of glucose, then this medium was replaced by fresh DMEM 1 g/L glucose. After 1 h, the supernatant was collected and frozen at -20°C, and the high-glucose (4.5 g/L) DMEM solution was added to the well. After 1 h, the supernatant was collected and the islets were lysed in each well using RIPA buffer (50 mM TRIS Euromedex 200923-A, 150 nM NaCl Euromedex 1112-A, 0.5% Sodium deoxycholate Sigma 30970, 1% IGEPAL CA-630 Sigma I8896, 1% SDS Sigma L3771) under agitation during 30 min at 4°C. The lysate was sampled and kept at -20°C for total protein measurement. Supernatants collected were kept at -20°C, then insulin was measured using the protocol below, and BCA assay (Thermo Scientific, 23227) was performed to normalize insulin secretion to total protein content.

2.3 Insulin measurement

Insulin levels were measured in samples kept at -20°C (for both blood serum and GSIS lysates), using Ultra Sensitive Insulin ELISA kit (Crystal Chem, 90080). Measurements were performed using instructions provided by the manufacturer.

2.4. Histological analysis

Pancreas were dissected and directly fixed in 4% paraformaldehyde overnight before embedding in paraplast (Paraplast X-tra, 39603002, Leica). 6 µm-thick sections were produced, and antigen retrieval was performed in sodium citrate buffer at 100°C before staining. For immunofluorescence staining, 2 different sections per mouse spaced by at least 120 µm were

co-stained with rabbit anti-insulin (1:500, Thermofisher, bs-0056R) and mouse anti-glucagon (1:500, Abcam, ab10922) primary antibodies overnight at 4°C followed with a 1-hour incubation with the secondary antibodies Alexa Fluor 555 donkey anti-rabbit (1:400, Invitrogen, A21428) and Alexa Fluor 488 goat anti-mouse IgG1 (1:500, Invitrogen, 121121) at room temperature. Image acquisitions were realized using Leica DM6000 upright epifluorescence microscope, with a 10x objective (HC PL APO 10X/0.4 (NA), Phase 1/2, 2 mm (WD)). Post-acquisition image analysis was performed with Fiji software [27]. For islet counts, 4 mice per condition were analyzed.

2.5. Somatotropic axis phenotyping

Frozen liver samples were processed for western blot as described by Schwarzer et al. [28]. Briefly, livers were lysed in RIPA Plus lysis buffer, protein concentration was measured with BCA assay, and 30 µg protein were loaded per well in Mini-PROTEAN TGX Stain Free precast gels (Bio-Rad, 4868096). Proteins were transferred to nitrocellulose membranes using Trans-Blot Turbo system (Bio-Rad). Membranes were blocked, incubated with rabbit monoclonal anti-total Akt (C67E7) (1:1,000, Cell Signaling, #4691) or rabbit monoclonal anti-phospho S473 Akt (D9E) (1:2,000, Cell signaling, #4060) for 1 hour at room temperature, washed, and incubated with anti-Rabbit IgG, HRP Conjugate (1:2,500, Promega, W4011) secondary antibody for 1 hour at room temperature. After washing, revelation was done by incubation with ECL Western Blotting Substrate (Promega, W1001). Signals were recorded with Amersham IQ800 imager (Cytiva). Image analysis was performed in Image Lab software version 6.1 (Bio-Rad) using total protein normalization [29].

For liver IGF-1 measurement, liver tissues were weighed and homogenized in lysis buffer containing PBS, 1% Triton X100 and a protease inhibitor mixture (Roche, cOmplete™, EDTA-free Protease Inhibitor Cocktail). After centrifugation (12,000 x g for 10 minutes, 4°C), supernatants were collected and used to measure IGF-1 levels by Mouse/Rat IGF-1 Quantikine ELISA (R&D systems, MG100). BCA assay was performed to normalize IGF-1 concentration to protein concentration in the liver. Results are expressed as pg/µg of protein.

For RT-qPCRs, total RNA was extracted from liver and muscle using Nucleospin RNA kit (Macherey-Nagel, 740955.250), then reverse transcription was performed on 1 µg of RNA using SensiFAST cDNA synthesis Kit (Meridian Biosciences, BIO-65053). Quantitative PCR was performed with Takyon NO ROX SYBR Mastermix blue dTTP (Eurogentec, UF-NSMT-B0701) using a Bio-Rad CFX96 apparatus. Analysis was performed according to the MIQE guidelines [30]. At least two control genes were used for each tissue to determine relative expression of target genes, after confirming stability of the genes using the geNorm tool available within the

CFX96 software. Primers for control and target genes are listed in Table 2. Data are expressed as geometric mean relative to the expression of the control genes.

2.6. RNA-seq analysis

Concentration and quality of the 10 DNAse-treated RNA samples were assessed using Qubit 4.0 (Thermo Fisher Scientific) and Tapestation 4150 (Agilent Technologies), respectively. First, for each sample, mRNA purification, based on oligo dT-based mRNA isolation, was conducted with a starting material of 1µg of total RNA using the Poly(A) mRNA Magnetic Isolation Module (New England Biolabs) and following the manufacturer's instructions. Then, single-indexed libraries were built using the CORALL Total RNA-Seq Library Prep Kit (Lexogen) and following the manufacturer's instructions. This fragmentation-free protocol provides for complete transcript coverage. Moreover, Lexogen protocol integrates Unique Molecular Identifiers (UMIs, 12bp tags) added during the linker Ligation step before amplification. It can be used to reduce errors and quantitative bias introduced by the amplification. After quality control based on Qubit 4.0 and Tapestation analysis, libraries were pooled together in an equimolar manner and sequenced on two high-output runs in a single-end mode (1×86 bp) using a NextSeq500 Illumina sequencer. A total of 1.082 billion reads were generated, resulting after demultiplexing in an average of 36 million reads per sample, with 31 to 44 million reads per sample.

Reads were then analyzed using a local pipeline derived from the one supported by Lexogen. Briefly, adapter sequences were first removed using the Cutadapt package (version 3.5) [31] and quality control of reads was performed using FastQC. Read mapping was achieved with STAR (Spliced Transcripts Alignment to a Reference, version 2.7.11a) [32] using the *Mus musculus* GRCm39 genome reference (Ensembl, release 110). Umi_tools dedup (version 1.1.2) [33] was conducted to UMI deduplication, enabling the accurate bioinformatic identification of PCR duplicates. The mapped reads were then quantified by htseq-count (version 2.0.3) [34] allowing to generate a count table by sample. From the count tables, R software v.4.3.1 was used to perform differential expression analysis using Deseq2 v.1.42.0 package [35]. Enhanced Volcano v.1.20.0 package [36] was used to represent differential expression data, using selective cut-offs of adjusted (by False Discovery Rate correction) p-value $p \leq 0.01$, with a restriction to fold-change (FC) such that $|\log_2 FC| \geq 1$. PCA plot was created using PCA tools v.2.14.0 package [37]. Gene Ontology [38], [39] terms enrichment analysis was performed using cluster Profiler v.4.10.0 package [40]. Genes found in upregulated GO term analysis were represented in a heatmap created with Complex Heatmaps v.2.18.0 package [41]. After quality check and unsupervised analysis, one sample from a LPD mouse treated with vehicle appeared to be an outlier and was therefore excluded from analysis.

2.7. Statistical analysis

Statistical analysis was performed using Graphpad Prism v10.2.1. ANOVA-2 results are listed in Table 3.

2. **Results and discussion**:

3.1. Chronic semaglutide treatment improves glucose tolerance, irrespective of the diet

To determine the effects of chronic semaglutide treatment during juvenile malnutrition, we first characterized glucose metabolism of malnourished (LPD, 5% protein) and control (CD, 20% protein) juvenile male mice (Figure 1A). As previously described [21], [22], [23], [42], chronic protein malnutrition triggered a decrease in fasting glycemia (Figure 1B) and fasting insulinemia (Figure 1C). However, chronic semaglutide treatment did not further alter these parameters in LPD nor CD mice (Table 2), contrary to what has been described in mouse models of obesity [43]. Conversely, semaglutide markedly improved glucose tolerance, as assessed by oral glucose tolerance test in both dietary conditions (Figures 1D-E). Surprisingly, in our model, semaglutide did not potentiate systemic insulin production (Figures 1F).

3.2. Semaglutide remodels pancreatic islet physiology in a diet-dependent manner

To explore the mechanisms underlying semaglutide-mediated improvement of glucose tolerance in both dietary conditions, we examined the morphology of pancreatic islets of CD and LPD mice treated with semaglutide or vehicle. Strikingly, semaglutide treatment induced a reduction in the mean islet area of CD, but not LPD animals (Figure 1G-H), suggesting that semaglutide regulates the development of pancreatic islets in a diet-dependent manner. Our data in CD animals are in line with a previous study showing that semaglutide triggers a reduction in pancreatic islet area in both AIN93 and high fat-fed adult mice [44]. In addition, *ex vivo* assessment of the ability of pancreatic islets to secrete insulin in response to glucose stimulation demonstrated that semaglutide potentiates insulin secretion from isolated islets from LPD but not CD animals (Figure 1I). Interestingly, previous studies have shown that pancreatic islets from diet-induced obese adult mice display decreased glucose-stimulated insulin secretion when treated with semaglutide, while no effect of semaglutide was detected on the islets of AIN93-fed mice [44]. These data further emphasize a specific effect of semaglutide on pancreatic islet physiology during malnutrition. However, semaglutide-mediated potentiation of insulin secretion was only detected *ex vivo*, and does not explain circulating insulin levels in response to an oral glucose tolerance test (Figure 1D-E). The differential response between *ex vivo* and *in vivo* experiments suggests additional mechanisms in LPD mice, which would also participate in glucose tolerance improvement. Indeed, in addition to pancreatic beta cells, semaglutide signals to various other cell types expressing the GLP-1 receptor [45], [46], which could trigger additional physiological responses. For example, recent data suggest that many of GLP-1RA effects – including appetite regulation and weight loss – could be mediated by brain

cells expressing the GLP-1 receptor [47]. Besides, GLP-1 and GLP-1RAs can interact with other signaling pathways [15]. Indeed, it has recently been proven that GLP-1 can directly bind to and activate the IGF-1R [13]. Given the massive growth and IGF-1 activity alterations induced by juvenile malnutrition, this prompted us to examine the effects of semaglutide on growth of malnourished juvenile animals.

3.3. Chronic semaglutide treatment further compromises linear growth of malnourished juvenile mice

Low protein feeding during the juvenile period severely altered macroscopic growth parameters, with LPD mice being on average 14% shorter and 30% lighter than CD animals (Figure 2A-F). While chronic semaglutide treatment did not significantly alter these parameters in control mice, it drastically impaired the growth of malnourished animals. Indeed, LPD mice treated with semaglutide were 7% shorter and 32% lighter than vehicle-treated animals, displaying a 3.5-fold reduction in linear growth rate, and a consistent reduction in leg bone size (Figure 2A-F).

Semaglutide is now widely used for its efficacy in inducing weight loss, notably by decreasing food intake both in obese humans [5], [6] and mice [48]. Surprisingly, semaglutide treatment did not alter food intake in CD nor LPD animals (Fig 2G), indicating that semaglutide-mediated growth alterations in LPD mice were not related to decreased energy intake. Furthermore, semaglutide-treated LPD mice displayed decreased weight of fat but not lean organs (Figure 2H-K). In CD animals, semaglutide did not affect the weight of fat and lean organs, indicating a specific effect of semaglutide on fat storage during malnutrition.

Altogether, these data highlight a diet-dependent effect of semaglutide treatment on linear growth. The effects of semaglutide during the juvenile period have been poorly investigated in rodents. Indeed, to our knowledge only one study probed the effects of semaglutide after weaning, in a model of infantile neuroaxonal dystrophy, and did not report any interference of semaglutide with the growth of chow diet-fed mice [49]. This is consistent with our data in CD mice. Consistently, the GLP-1RAs semaglutide and liraglutide had no reported effect on growth during trials in adolescents with obesity [7], [50], [51]. Therefore, the surprising phenotype that we observed in LPD mice incited us to further explore the mechanisms by which semaglutide interferes with linear growth.

3.4. Semaglutide does not affect growth changes in malnourished juveniles through the somatotropic axis

In mammals, the main determinant of linear growth is the GH/IGF-1 axis (Figure 3A), whose activity is altered upon poor nutrition [28], [52]. Consistent with previous studies, LPD mice had reduced levels of circulating IGF-1 (Figure 3B, Table 3), concomitant with decreased liver *Igf1* expression (Figure 3C, Table 3) and production (Figure 3D, Table 3). In addition, *Ghr* expression was decreased in the liver of LPD animals (Figure 3E, Table 3), consistent with a

GH-resistant state [53]. Surprisingly, none of these parameters was further altered in semaglutide-treated LPD mice, suggesting that semaglutide does not enhance GH resistance nor further impairs IGF-1 production upon chronic protein malnutrition.

Since GLP-1 and GLP-1RAs can interfere with IGF-1 signaling by modulating IGF-1R expression [10], [11] and interacting with IGF-1R [13], we hypothesized that semaglutide-treated LPD mice could develop a resistance to IGF-1 in addition to their resistance to GH, which could explain their hampered growth. A major target tissue of IGF-1-mediated growth is the skeletal muscle, where IGF-1 signaling notably stimulates anabolism [54]. Our data showed no effect of semaglutide treatment on muscle *Igf1r* expression (Figure 3 F). We assessed phosphorylation of the Akt kinase, a downstream target of IGF-1R, and observed an increased activation of the IGF-1 signaling pathway in the muscle of semaglutide-treated CD mice (Figure 3F-G). Surprisingly this was independent of increased muscle mass or linear growth (Fig 2A-D, 2K), and of any other effect of semaglutide treatment on the somatotropic growth axis of CD mice (Fig 3B-E). Interestingly, semaglutide treatment did not alter the ratio of phosphorylated versus total Akt in LPD mice, thus invalidating our hypothesis of semaglutide-induced IGF-1 resistance in the muscle of these animals. Therefore, semaglutide does not seem to further interfere with the somatotropic axis of malnourished animals.

3.5. Liver transcriptome shows signatures of altered circadian clock and thermogenesis in semaglutide-treated malnourished mice

The liver has a central role in both growth and energy homeostasis, two key processes that are altered by semaglutide treatment in malnourished juveniles. Therefore, to gain better insights into the molecular mechanisms underpinning these semaglutide-mediated phenotypes, we performed transcriptomic analysis of the liver of semaglutide and vehicle-treated LPD mice.

There were significant changes in the liver transcriptome in response to semaglutide, as shown by separated clustering of the two groups of samples (Figure 4A). However, in total only 126 genes (out of nearly 13,000 detected genes) were differentially regulated in semaglutide-compared to vehicle-treated LPD mice (47 upregulated, 79 downregulated), revealing mild remodeling of the liver transcriptome upon semaglutide treatment (Figure 4B).

To better understand the functions impacted by those changes, we performed a gene ontology terms enrichment analysis among the genes upregulated by semaglutide treatment in LPD mice. Among the 11 enriched GO terms in semaglutide treated-mice, 7 referred to circadian rhythm and 3 were related to thermogenesis (Figure 4C). Consistently, major clock genes such as *Per* genes, *Usp2*, *Ciart* and *Id1* were upregulated by semaglutide treatment (Figure 4D). Similarly, genes involved in thermogenic processes (*Ffar4, Lepr, Map2k6, Adrb2*) had increased expression in the liver of semaglutide-treated mice.

To our knowledge, our study is the first associating semaglutide treatment with transcriptomic signatures relating to alterations of the circadian rhythm. However, many studies have

described that in type 2 diabetes or obesity, semaglutide can lead to a modification of food intake patterns, a process that is tightly regulated in a circadian manner [55]. In addition, the secretion pattern of endogenous GLP-1 is circadian in healthy conditions [56], [57]. Therefore, treating animals with a long-lasting GLP-1 receptor agonist might perturbate the rhythmicity of GLP-1 signaling.

Our transcriptomic data indicate a remodeling of the LPD liver transcriptome in response to semaglutide (Fig 4). However, several studies have reported the absence of GLP-1 receptors in hepatocytes in rodents [45], [58], monkeys and humans [46]. In line with this, we did not see any significant expression of GLP-1R in our transcriptomic data. This indicates that the hepatic effects of semaglutide are probably not the reflect of direct action of semaglutide on hepatocytes. Alternatively, it has been suggested that the targets of GLP-1RAs in the liver could rather be infiltrating immune cells [59]. In addition, several studies have shown that some of the physiological effects of GLP-1RAs could be mediated by their capacity to stimulate hepatic Fibroblast Growth Factor 21 (FGF21) production and responsiveness [60], [61], [62]. It is well described that FGF21 expression is induced by protein malnutrition [63]. We did not detect differential expression of *Fgf21* in our LPD mice liver transcriptome dataset, suggesting that semaglutide modulates the physiology of LPD mice independently of this pathway.

Our gene ontology enrichment analysis evidenced that both circadian rhythm and thermogenesis were altered in the liver of semaglutide-treated LPD mice. These two processes are intricately correlated because circadian rhythm plays a pivotal role in regulating body heat production [64]. Therefore, the alteration of these two processes might be the expression of the same biological phenomenon. Changes in thermogenesis could provide a hypothesis for semaglutide-mediated growth impairment in LPD animals. Indeed, semaglutide administration in LPD mice may lead to an increase in heat production and thus in the overall energy expenditure of the organism. Therefore, it is likely that semaglutide-treated LPD mice exhibit reduced energy allocation towards linear growth compared to vehicle-treated animals. Consistent with this idea, semaglutide-mediated enhancement of energy expenditure has been described in obese mice [48]. However, human data do not align with this pattern [65], emphasizing that the effects of semaglutide on energy expenditure are highly dependent on the nutritional and experimental context. Moreover, semaglutide can stimulate the browning of subcutaneous fat adipocytes in obese mice [66], a process that could participate in the putative increase in thermogenesis induced by semaglutide in malnourished mice.

4. Conclusions

Comprehending the potential impacts of the increasingly prevalent GLP-1RA semaglutide use in the clinic is essential to guarantee its safe and effective utilization. No deleterious effects of GLP-1RAs on growth of obese children and adolescents were reported so far [7], [50], [51], [67]. However, here we demonstrate that semaglutide differentially interacts with the physiology of

juvenile mice depending on their dietary protein intake. We found that semaglutide distinctively modifies pancreatic islet physiology and morphology depending on the diet. Importantly, our study demonstrates an effect of semaglutide on murine linear growth, with semaglutide drastically hampering the growth of protein malnourished, but not control-fed, animals. The mechanisms of this semaglutide-mediated linear growth impairment are not dependent on the GH/IGF-1 axis and remain to be fully uncovered. Yet our liver transcriptomic results indicate that semaglutide may enhance thermogenesis and alter the circadian rhythm of malnourished mice, preventing energy investment in linear growth, anabolism and fat storage. Our study highlights an unexpected consequence of semaglutide treatment in a preclinical model of juvenile protein malnutrition, suggesting caution is warranted when using GLP-1RAs in low protein-intake infants prone to metabolic disorders. Our results pave the way for future studies to investigate the mechanisms of action of GLP-1RAs comprehensively in order to understand how they affect energy metabolism and linear growth during protein malnutrition.

Bibliography:

[1] H. Yao *et al.*, “Comparative effectiveness of GLP-1 receptor agonists on glycaemic control, body weight, and lipid profile for type 2 diabetes: systematic review and network meta-analysis,” *The BMJ*, vol. 384, p. e076410, Jan. 2024, doi: 10.1136/bmj-2023-076410.

[2] J. Lau *et al.*, “Discovery of the Once-Weekly Glucagon-Like Peptide-1 (GLP-1) Analogue Semaglutide,” *J. Med. Chem.*, vol. 58, no. 18, pp. 7370–7380, Sep. 2015, doi: 10.1021/acs.jmedchem.5b00726.

[3] C. Kapitza, K. Dahl, J. B. Jacobsen, M. B. Axelsen, and A. Flint, “Effects of semaglutide on beta cell function and glycaemic control in participants with type 2 diabetes: a randomised, double-blind, placebo-controlled trial,” *Diabetologia*, vol. 60, no. 8, pp. 1390–1399, 2017, doi: 10.1007/s00125-017-4289-0.

[4] J. Blundell *et al.*, “Effects of once□weekly semaglutide on appetite, energy intake, control of eating, food preference and body weight in subjects with obesity,” *Diabetes Obes. Metab.*, vol. 19, no. 9, pp. 1242–1251, Sep. 2017, doi: 10.1111/dom.12932.

[5] J. P. H. Wilding *et al.*, “Once-Weekly Semaglutide in Adults with Overweight or Obesity,” *N. Engl. J. Med.*, vol. 384, no. 11, pp. 989–1002, Mar. 2021, doi: 10.1056/NEJMoa2032183.

[6] X. Gao *et al.*, “Efficacy and safety of semaglutide on weight loss in obese or overweight patients without diabetes: A systematic review and meta-analysis of randomized controlled trials,” *Front. Pharmacol.*, vol. 13, Sep. 2022, doi: 10.3389/fphar.2022.935823.

[7] D. Weghuber *et al.*, “Once-Weekly Semaglutide in Adolescents with Obesity,” *N. Engl. J. Med.*, vol. 387, no. 24, pp. 2245–2257, Dec. 2022, doi: 10.1056/NEJMoa2208601.

[8] M. Zhang *et al.*, “Exendin-4 enhances proliferation of senescent osteoblasts through activation of the IGF-1/IGF-1R signaling pathway,” *Biochem. Biophys. Res. Commun.*, vol. 516, no. 1, pp. 300–306, Aug. 2019, doi: 10.1016/j.bbrc.2019.06.112.

[9] X. Ma *et al.*, “Exendin□4, a Glucagon□Like Peptide□1 Receptor Agonist, Prevents Osteopenia by Promoting Bone Formation and Suppressing Bone Resorption in Aged Ovariectomized Rats,” *J. Bone Miner. Res.*, vol. 28, no. 7, pp. 1641–1652, Jul. 2013, doi: 10.1002/jbmr.1898.

[10] M. Cornu, J.-Y. Yang, E. Jaccard, C. Poussin, C. Widmann, and B. Thorens, “Glucagon-like peptide-1 protects beta-cells against apoptosis by increasing the activity of an IGF-2/IGF-1 receptor autocrine loop,” *Diabetes*, vol. 58, no. 8, pp. 1816–1825, Aug. 2009, doi: 10.2337/db09-0063.

[11] M. Arakawa *et al.*, “Effects of exendin-4 on glucose tolerance, insulin secretion, and beta-cell proliferation depend on treatment dose, treatment duration and meal contents,” *Biochem. Biophys. Res. Commun.*, vol. 390, no. 3, pp. 809–814, Dec. 2009, doi: 10.1016/j.bbrc.2009.10.054.

[12] C. Yamada *et al.*, “The murine glucagon-like peptide-1 receptor is essential for control of bone resorption,” *Endocrinology*, vol. 149, no. 2, pp. 574–579, Feb. 2008, doi: 10.1210/en.2007-1292.

[13] N. Qa’aty *et al.*, “The Antidiabetic Hormone Glucagon-Like Peptide-1 Induces Formation of New Elastic Fibers in Human Cardiac Fibroblasts After Cross-Activation of IGF-IR,” *Endocrinology*, vol. 156, no. 1, pp. 90–102, Jan. 2015, doi: 10.1210/en.2014-1519.

[14] K. Heinla, E. Vasar, I. Reppo, T. Sedman, and V. Volke, “GLP-1 Receptor Agonists Induce Growth Hormone Secretion in Healthy Volunteers,” *Diabetes Ther. Res. Treat. Educ. Diabetes Relat. Disord.*, vol. 14, no. 4, pp. 777–786, Apr. 2023, doi: 10.1007/s13300-023-01381-w.

[15] A. Cignarelli *et al.*, “Mini Review: Effect of GLP-1 Receptor Agonists and SGLT-2 Inhibitors on the Growth Hormone/IGF Axis,” *Front. Endocrinol.*, vol. 13, Feb. 2022, doi: 10.3389/fendo.2022.846903.

[16] P. A. Martins and A. L. Sawaya, “Evidence for impaired insulin production and higher sensitivity in stunted children living in slums,” *Br. J. Nutr.*, vol. 95, no. 5, pp. 996–1001, May 2006, doi: 10.1079/BJN20061754.

[17] M. N. Spoelstra *et al.*, “Kwashiorkor and marasmus are both associated with impaired glucose clearance related to pancreatic β-cell dysfunction,” *Metabolism*, vol. 61, no. 9, pp. 1224–1230, Sep. 2012, doi: 10.1016/j.metabol.2012.01.019.

[18] G. A. O. Alleyne, P. M. Trust, H. Flores, and H. Robinson, “Glucose tolerance and insulin sensitivity in malnourished children,” *Br. J. Nutr.*, vol. 27, no. 3, pp. 585–592, May 1972, doi: 10.1079/BJN19720128.

[19] R. H. J. Bandsma *et al.*, “Mechanisms behind decreased endogenous glucose production in malnourished children:,” *Pediatr. Res.*, p. 1, Jul. 2010, doi: 10.1203/PDR.0b013e3181f2b959.

[20] M. de Onis and F. Branca, “Childhood stunting: a global perspective: Childhood stunting: a global perspective,” *Matern. Child. Nutr.*, vol. 12, pp. 12–26, May 2016, doi: 10.1111/mcn.12231.

[21] M. Schwarzer *et al.*, “Microbe-mediated intestinal NOD2 stimulation improves linear growth of undernourished infant mice,” *Science*, vol. 379, no. 6634, pp. 826–833, Feb. 2023, doi: 10.1126/science.ade9767.

[22] S. Soriano *et al.*, “Reduced Insulin Secretion in Protein Malnourished Mice Is Associated with Multiple Changes in the β-Cell Stimulus-Secretion Coupling,” *Endocrinology*, vol. 151, no. 8, pp. 3543–3554, Aug. 2010, doi: 10.1210/en.2010-0008.

[23] P. C. Borck *et al.*, “Protein malnutrition after weaning disrupts peripheral clock and daily insulin secretion in mice,” *J. Nutr. Biochem.*, vol. 50, pp. 54–65, Dec. 2017, doi: 10.1016/j.jnutbio.2017.08.013.

[24] J.-L. Thoumas, A. Cavaroc, D. Sery, F. Leulier, and F. D. Vadder, “Suboptimal refeeding compensates stunting in a mouse model of juvenile malnutrition.” bioRxiv, p. 2024.03.25.586077, Mar. 25, 2024. doi: 10.1101/2024.03.25.586077.

[25] D.-S. Li, Y.-H. Yuan, H.-J. Tu, Q.-L. Liang, and L.-J. Dai, “A protocol for islet isolation from mouse pancreas,” *Nat. Protoc.*, vol. 4, no. 11, Art. no. 11, Nov. 2009, doi: 10.1038/nprot.2009.150.

[26] Y.-X. Zhu, Y.-C. Zhou, Y. Zhang, P. Sun, X.-A. Chang, and X. Han, “Protocol for in vivo and ex vivo assessments of glucose-stimulated insulin secretion in mouse islet β cells,” *STAR Protoc.*, vol. 2, no. 3, p. 100728, Sep. 2021, doi: 10.1016/j.xpro.2021.100728.

[27] J. Schindelin *et al.*, “Fiji: an open-source platform for biological-image analysis,” *Nat. Methods*, vol. 9, no. 7, Art. no. 7, Jul. 2012, doi: 10.1038/nmeth.2019.

[28] M. Schwarzer *et al.*, “Lactobacillus plantarum strain maintains growth of infant mice during chronic undernutrition,” *Science*, vol. 351, no. 6275, pp. 854–857, Feb. 2016, doi: 10.1126/science.aad8588.

[29] A. J. Fosang and R. J. Colbran, “Transparency Is the Key to Quality,” *J. Biol. Chem.*, vol. 290, no. 50, p. 29692, Dec. 2015, doi: 10.1074/jbc.E115.000002.

[30] S. A. Bustin *et al.*, “The MIQE guidelines: minimum information for publication of quantitative real-time PCR experiments,” *Clin. Chem.*, vol. 55, no. 4, pp. 611–622, Apr. 2009, doi: 10.1373/clinchem.2008.112797.

[31] M. Martin, “Cutadapt removes adapter sequences from high-throughput sequencing reads,” *EMBnet.journal*, vol. 17, no. 1, Art. no. 1, May 2011, doi: 10.14806/ej.17.1.200.

[32] A. Dobin *et al.*, “STAR: ultrafast universal RNA-seq aligner,” *Bioinforma. Oxf. Engl.*, vol. 29, no. 1, pp. 15–21, Jan. 2013, doi: 10.1093/bioinformatics/bts635.

[33] T. Smith, A. Heger, and I. Sudbery, “UMI-tools: modeling sequencing errors in Unique Molecular Identifiers to improve quantification accuracy,” *Genome Res.*, vol. 27, no. 3, pp. 491–499,

Mar. 2017, doi: 10.1101/gr.209601.116.

[34] S. Anders, P. T. Pyl, and W. Huber, “HTSeq--a Python framework to work with high-throughput sequencing data,” *Bioinforma. Oxf. Engl.*, vol. 31, no. 2, pp. 166–169, Jan. 2015, doi: 10.1093/bioinformatics/btu638.

[35] M. I. Love, W. Huber, and S. Anders, “Moderated estimation of fold change and dispersion for RNA-seq data with DESeq2,” *Genome Biol.*, vol. 15, no. 12, p. 550, Dec. 2014, doi: 10.1186/s13059-014-0550-8.

[36] K. Blighe, S. Rana, and M. Lewis, “EnhancedVolcano: Publication-ready volcano plots with enhanced colouring and labeling.” 2023. doi: 10.18129/B9.BIOC.ENHANCEDVOLCANO.

[37] K. Blighe and A. Lun, “PCAtools: PCAtools: Everything Principal Components Analysis.” 2023. doi: 10.18129/B9.bioc.PCAtools.

[38] M. Ashburner *et al.*, “Gene Ontology: tool for the unification of biology,” *Nat. Genet.*, vol. 25, no. 1, Art. no. 1, May 2000, doi: 10.1038/75556.

[39] T. G. O. Consortium *et al.*, “The Gene Ontology knowledgebase in 2023,” *Genetics*, vol. 224, no. 1, May 2023, doi: 10.1093/genetics/iyad031.

[40] T. Wu *et al.*, “clusterProfiler 4.0: A universal enrichment tool for interpreting omics data,” *The Innovation*, vol. 2, no. 3, p. 100141, Aug. 2021, doi: 10.1016/j.xinn.2021.100141.

[41] Z. Gu, R. Eils, and M. Schlesner, “Complex heatmaps reveal patterns and correlations in multidimensional genomic data,” *Bioinformatics*, vol. 32, no. 18, pp. 2847–2849, Sep. 2016, doi: 10.1093/bioinformatics/btw313.

[42] S. Aparecida De França *et al.*, “Low protein diet changes the energetic balance and sympathetic activity in brown adipose tissue of growing rats,” *Nutrition*, vol. 25, no. 11–12, pp. 1186–1192, Nov. 2009, doi: 10.1016/j.nut.2009.03.011.

[43] S. Niu *et al.*, “Semaglutide ameliorates metabolism and hepatic outcomes in an NAFLD mouse model,” *Front. Endocrinol.*, vol. 13, p. 1046130, Dec. 2022, doi: 10.3389/fendo.2022.1046130.

[44] T. de S. Marinho, F. F. Martins, L. E. de M. Cardoso, M. B. Aguila, and C. A. Mandarim-de-Lacerda, “Pancreatic islet cells disarray, apoptosis, and proliferation in obese mice. The role of Semaglutide treatment,” *Biochimie*, vol. 193, pp. 126–136, Feb. 2022, doi: 10.1016/j.biochi.2021.10.017.

[45] B. P. Bullock, R. S. Heller, and J. F. Habener, “Tissue distribution of messenger ribonucleic acid encoding the rat glucagon-like peptide-1 receptor,” *Endocrinology*, vol. 137, no. 7, pp. 2968–2978, Jul. 1996, doi: 10.1210/endo.137.7.8770921.

[46] C. Pyke *et al.*, “GLP-1 receptor localization in monkey and human tissue: novel distribution revealed with extensively validated monoclonal antibody,” *Endocrinology*, vol. 155, no. 4, pp. 1280–1290, Apr. 2014, doi: 10.1210/en.2013-1934.

[47] S. Buller and C. Blouet, “Brain access of incretins and incretin receptor agonists to their central targets relevant for appetite suppression and weight loss,” *Am. J. Physiol.-Endocrinol. Metab.*, vol. 326, no. 4, pp. E472–E480, Apr. 2024, doi: 10.1152/ajpendo.00250.2023.

[48] S. Gabery *et al.*, “Semaglutide lowers body weight in rodents via distributed neural pathways,” *JCI Insight*, vol. 5, no. 6, pp. e133429, 133429, Mar. 2020, doi: 10.1172/jci.insight.133429.

[49] L. Poupon-Bejuit *et al.*, “A GLP1 receptor agonist diabetes drug ameliorates neurodegeneration in a mouse model of infantile neurometabolic disease,” *Sci. Rep.*, vol. 12, p. 13825, Aug. 2022, doi: 10.1038/s41598-022-17338-1.

[50] Kelly Aaron S. *et al.*, “A Randomized, Controlled Trial of Liraglutide for Adolescents with Obesity,” *N. Engl. J. Med.*, vol. 382, no. 22, pp. 2117–2128, May 2020, doi: 10.1056/NEJMoa1916038.

[51] G. Diene *et al.*, “Liraglutide for Weight Management in Children and Adolescents With Prader–Willi Syndrome and Obesity,” *J. Clin. Endocrinol. Metab.*, vol. 108, no. 1, pp. 4–12, Jan. 2023, doi: 10.1210/clinem/dgac549.

[52] J.-L. Liu and D. LeRoith, “Insulin-Like Growth Factor I Is Essential for Postnatal Growth in Response to Growth Hormone,” *Endocrinology*, vol. 140, no. 11, pp. 5178–5184, Nov. 1999, doi: 10.1210/endo.140.11.7151.

[53] P. K. Fazeli and A. Klibanski, “Determinants of GH resistance in malnutrition,” *J. Endocrinol.*, vol. 220, no. 3, pp. R57–R65, Mar. 2014, doi: 10.1530/JOE-13-0477.

[54] T. Shavlakadze *et al.*, “A growth stimulus is needed for IGF-1 to induce skeletal muscle hypertrophy in vivo,” *J. Cell Sci.*, vol. 126, no. 19, pp. 4536–4536, Oct. 2013, doi: 10.1242/jcs.141143.

[55] S. Bettadapura, K. Dowling, K. Jablon, A. W. Al-Humadi, and C. W. le Roux, “Changes in food preferences and ingestive behaviors after glucagon-like peptide-1 analog treatment: techniques and opportunities,” *Int. J. Obes.*, pp. 1–9, Mar. 2024, doi: 10.1038/s41366-024-01500-y.

[56] C. Liu, Y. Liu, Y. Xin, and Y. Wang, “Circadian secretion rhythm of GLP-1 and its influencing factors,” *Front. Endocrinol.*, vol. 13, p. 991397, Dec. 2022, doi: 10.3389/fendo.2022.991397.

[57] A. D. Biancolin *et al.*, “The core clock gene, Bmal1, and its downstream target, the SNARE regulatory protein secretagogin, are necessary for circadian secretion of glucagon-like peptide-1,” *Mol. Metab.*, vol. 31, pp. 124–137, Jan. 2020, doi: 10.1016/j.molmet.2019.11.004.

[58] M. Guilliams *et al.*, “Spatial proteogenomics reveals distinct and evolutionarily conserved hepatic macrophage niches,” *Cell*, vol. 185, no. 2, pp. 379-396.e38, Jan. 2022, doi: 10.1016/j.cell.2021.12.018.

[59] H. H. Hansen *et al.*, “Semaglutide reduces tumor burden in the GAN diet-induced obese and biopsy-confirmed mouse model of NASH-HCC with advanced fibrosis,” *Sci. Rep.*, vol. 13, no. 1, p. 23056, Dec. 2023, doi: 10.1038/s41598-023-50328-5.

[60] J. Lee *et al.*, “Exendin-4 regulates lipid metabolism and fibroblast growth factor 21 in hepatic

steatosis," *Metabolism.*, vol. 63, no. 8, pp. 1041–1048, Aug. 2014, doi: 10.1016/j.metabol.2014.04.011.

[61] K. Nonogaki, M. Hazama, and N. Satoh, "Liraglutide suppresses obesity and hyperglycemia associated with increases in hepatic fibroblast growth factor 21 production in KKAy mice," *BioMed Res. Int.*, vol. 2014, p. 751930, 2014, doi: 10.1155/2014/751930.

[62] M. Yang *et al.*, "Liraglutide increases FGF-21 activity and insulin sensitivity in high fat diet and adiponectin knockdown induced insulin resistance," *PloS One*, vol. 7, no. 11, p. e48392, 2012, doi: 10.1371/journal.pone.0048392.

[63] T. Laeger *et al.*, "FGF21 is an endocrine signal of protein restriction," *J. Clin. Invest.*, vol. 124, no. 9, pp. 3913–3922, Sep. 2014, doi: 10.1172/JCI74915.

[64] M. E. Straat, R. Hogenboom, M. R. Boon, P. C. N. Rensen, and S. Kooijman, "Circadian control of brown adipose tissue," *Biochim. Biophys. Acta Mol. Cell Biol. Lipids*, vol. 1866, no. 8, p. 158961, Aug. 2021, doi: 10.1016/j.bbalip.2021.158961.

[65] M. A. Nauck, D. R. Quast, J. Wefers, and J. J. Meier, "GLP-1 receptor agonists in the treatment of type 2 diabetes - state-of-the-art," *Mol. Metab.*, vol. 46, p. 101102, Apr. 2021, doi: 10.1016/j.molmet.2020.101102.

[66] F. F. Martins *et al.*, "Semaglutide (GLP-1 receptor agonist) stimulates browning on subcutaneous fat adipocytes and mitigates inflammation and endoplasmic reticulum stress in visceral fat adipocytes of obese mice," *Cell Biochem. Funct.*, vol. 40, no. 8, pp. 903–913, 2022, doi: 10.1002/cbf.3751.

[67] Tamborlane William V. *et al.*, "Liraglutide in Children and Adolescents with Type 2 Diabetes," *N. Engl. J. Med.*, vol. 381, no. 7, pp. 637–646, Aug. 2019, doi: 10.1056/NEJMoa1903822.

[68] R. Edgar, "Gene Expression Omnibus: NCBI gene expression and hybridization array data repository," *Nucleic Acids Res.*, vol. 30, no. 1, pp. 207–210, Jan. 2002, doi: 10.1093/nar/30.1.207.

Figure captions

Figure 1. **Semaglutide treatment differentially affects glucose metabolism of malnourished and control animals**. (A) Experimental procedure; created with Biorender.com. (B-C) Fasting glycemia (B) and insulinemia (C) of male mice fed CD or LPD and treated with semaglutide or vehicle. (D-F) Glycemia in CD-fed (D) and LPD-fed mice (E) and insulinemia (F) during an oral glucose tolerance test performed at post-natal day 42 on male mice treated with semaglutide or vehicle. N = 7-8 mice per group. (G-H) Representative images of pancreatic islets stained for glucagon (cyan), insulin (magenta) and DAPI (grey) (G) and quantification of mean islet size (H). Each violin plot represents a single animal. A minimum of 33 islets per animal were measured. (I) Glucose-stimulated insulin secretion (GSIS) of isolated pancreatic islets from male mice fed CD or LPD and treated with semaglutide or vehicle. Data are represented as fold-change of secreted insulin in response to a glucose stimulation. LG: low glucose. HG: high glucose. Each dot represents a group of 10 islets isolated from a single animal.
Data are shown as mean ± SEM.
*$p < 0.05$, **$p < 0.01$; two-way ANOVA followed by Šidák's multiple comparisons test; ns: non statistically significant.

Figure 2. **Chronic semaglutide treatment hampers linear growth of malnourished but not control juvenile mice**. (A-F) Body length (A), growth rate (B), femur (C) and tibia size (D) at post-natal day 56; body weight (E) and weight gain (F) of CD- and LPD-fed animals treated with semaglutide or vehicle. (G) Cumulative food intake. (H-K) Weight of white adipose tissue (WAT) (H-I), liver (J) and soleus muscle (K) at post-natal day 56. Data are expressed as organ weight relative to total body weight, to account for body size differences in mice. N = 7-8 mice per group.
Data are shown as mean ± SEM.
*$p < 0.05$, **$p < 0.01$, ***$p < 0.001$, ****$p < 0.0001$; two-way ANOVA followed by Šidák's multiple comparisons test; ns: non statistically significant.

Figure 3. **Semaglutide treatment differentially interferes with the somatotropic axis of juvenile mice**. (A) Schematic of the growth hormone (GH)/insulin-like growth factor 1 (IGF-1) signaling pathway. Created with Biorender.com. (B-E) Serum IGF-1 concentration (B), liver *Igf1* expression (C), liver IGF-1 concentration (D) and liver *Ghr*

expression in male mice fed CD or LPD and treated with semaglutide or vehicle. (F-G) *Igf1r* expression (F) and phospho-S473-Akt versus total Akt ratio as quantified by western blot (G) in the soleus muscle of male mice fed CD or LPD and treated with semaglutide or vehicle. NaCl: vehicle, S: semaglutide. Quantification of the western blots was performed using total protein quantification.

Panels B, D and G: data are shown as mean ± SEM. Panels C, E and F: data are shown as geometric mean ± geometric SD.

**$p < 0.01$; two-way ANOVA followed by Šidák's multiple comparisons test; ns: non statistically significant.

Figure 4. **The liver transcriptome of juvenile malnourished mice indicates altered circadian rhythm and thermogenesis in response to chronic semaglutide treatment**. (A) Principal Component Analysis (PCA) on whole liver bulk RNA-sequencing data of LPD-fed mice treated with vehicle (black triangles) or semaglutide (pink circles). (B) Volcano plot representing results of differential expression analysis between vehicle- and semaglutide-treated LPD mice. Fold change represents differentially expressed genes in semaglutide, compared to vehicle-treated mice. (C) Gene Ontology (GO) term enrichment analysis on the list of differentially upregulated genes (right upper quarter of panel B). The count corresponds to the number of genes annotated with the associated GO term, the GeneRatio corresponds to the ratio between differentially expressed genes annotated with the GO term over the total number of genes differentially expressed, adjusted p-value is calculated using FDR. (D) Heatmap illustrating a subset of genes annotated with enriched GO terms in (C); each column corresponds to a single mouse treated with vehicle (black) or semaglutide (pink). (A-D) Vehicle-treated group is considered as control; N = 4 for vehicle-treated group, N = 5 for semaglutide-treated group.

Acknowledgements

The authors thank Benjamin Gillet and Sandrine Hughes from the sequencing platform of IGFL (PSI) for their help regarding the sequencing project. They also thank Raghav Galgali for his help in setting up the bioinformatics pipeline for transcriptomic data analysis, the animal facility of IGFL (PEHR) where animal experiments were conducted, and the associated group for animal welfare (SBEA).

Data accessibility

The RNA sequencing data have been deposited in NCBI's Gene Expression Omnibus [68] and are accessible through GEO Series accession number GSE266477 (https://www.ncbi.nlm.nih.gov/geo/query/acc.cgi?acc=GSE266477).

Funding

This work was supported by funding from Fondation pour la Recherche Médicale (Equipe FRM EQU202203014629), and the Agence Nationale de la Recherche (ANR PRC CE14 2024 "GutStunting"). AJ is supported by a grant from Fondation pour la Recherche Médicale (FDT202304016501) and LR is supported by a doctoral grant from the French Ministry of Research.

CRediT authorship contribution statement

AJ, LR, FL and FDV designed research; AJ and LR conducted animal experiments and bench research; YD and JD generated RNA sequencing data from biological samples; AJ, LR and FDV analyzed data; AJ, LR and FDV wrote the manuscript, which was reviewed by FL.

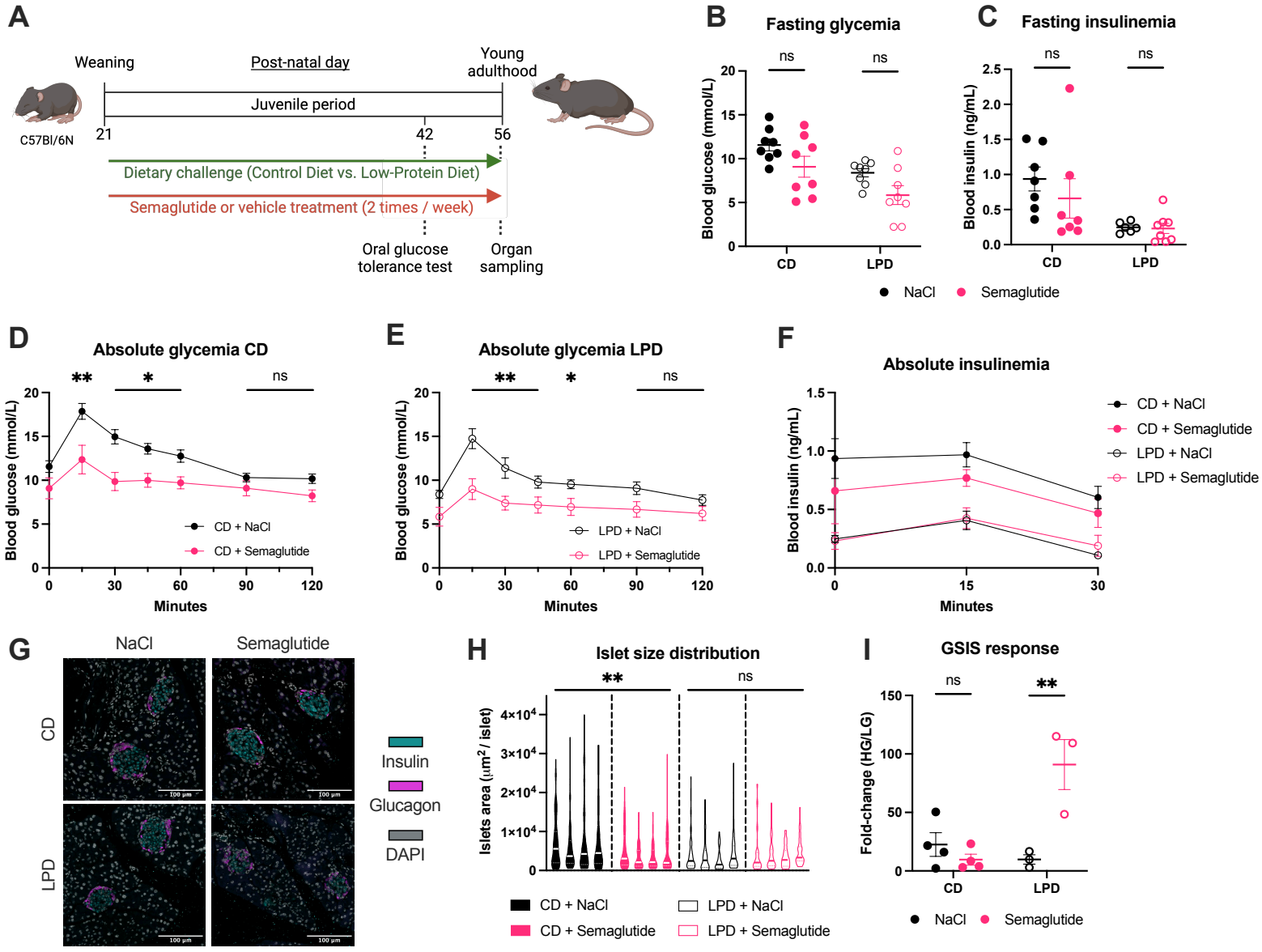
A
Weaning
Post-natal day
Young adulthood
Juvenile period
C57Bl/6N
21
42
56
Dietary challenge (Control Diet vs. Low-Protein Diet)
Semaglutide or vehicle treatment (2 times / week)
Oral glucose tolerance test
Organ sampling
B
Fasting glycemia
Blood glucose (mmol/L)
ns
CD
LPD
NaCl
Semaglutide
C
Fasting insulinemia
Blood insulin (ng/mL)
D
Absolute glycemia CD
Blood glucose (mmol/L)
Minutes
CD + NaCl
CD + Semaglutide
E
Absolute glycemia LPD
LPD + NaCl
LPD + Semaglutide
F
Absolute insulinemia
Blood insulin (ng/mL)
G
NaCl
Semaglutide
Insulin
Glucagon
DAPI
H
Islet size distribution
Islets area (µm² / islet)
I
GSIS response
Fold-change (HG/LG)

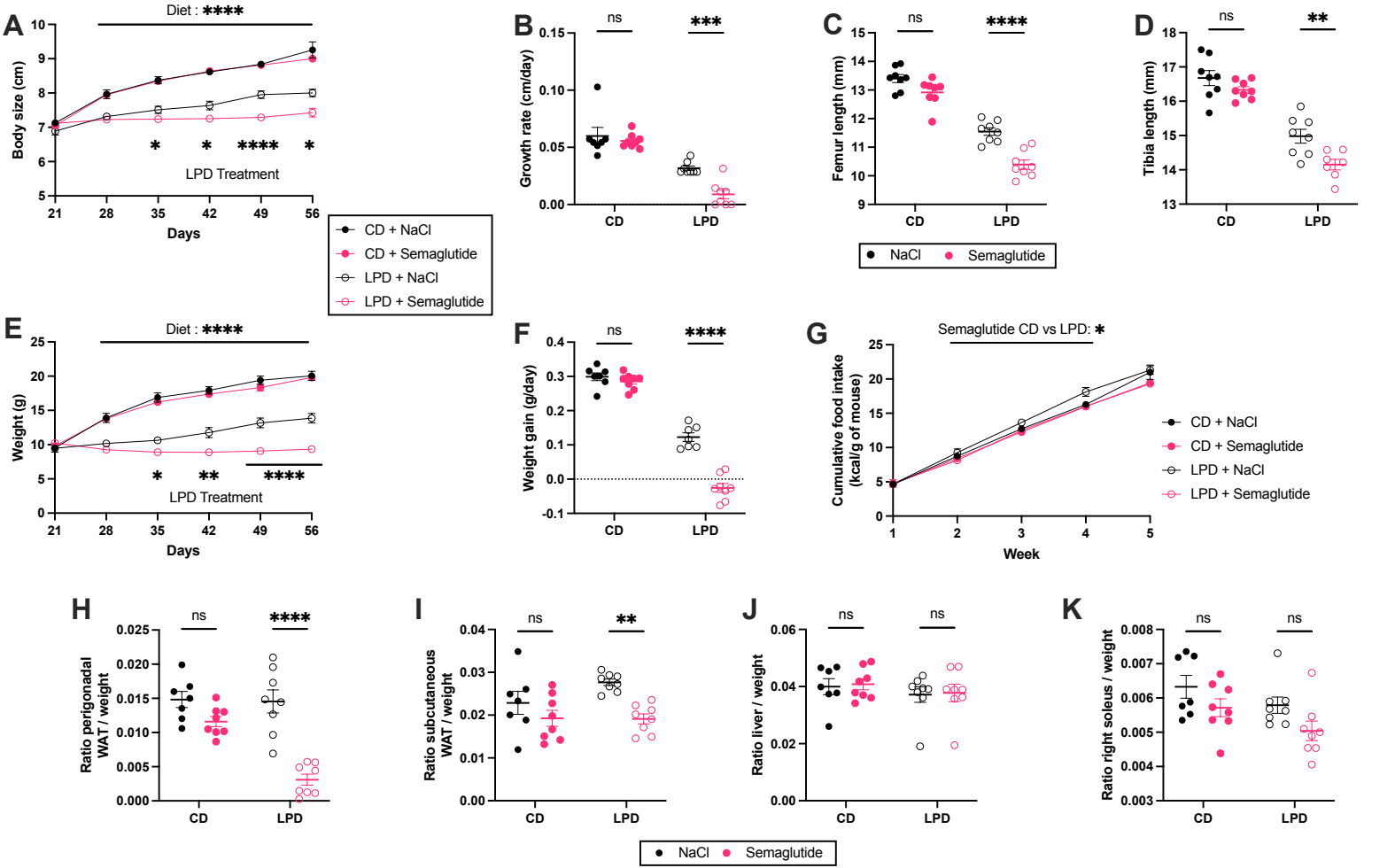
A
Diet : ****
Body size (cm)
LPD Treatment
Days
CD + NaCl
CD + Semaglutide
LPD + NaCl
LPD + Semaglutide
B
Growth rate (cm/day)
ns
***
CD
LPD
C
Femur length (mm)
ns
****
NaCl
Semaglutide
D
Tibia length (mm)
ns
**
E
Diet : ****
Weight (g)
LPD Treatment
Days
F
Weight gain (g/day)
ns
****
G
Semaglutide CD vs LPD: *
Cumulative food intake (kcal/g of mouse)
Week
H
Ratio perigonadal WAT / weight
I
Ratio subcutaneous WAT / weight
J
Ratio liver / weight
K
Ratio right soleus / weight

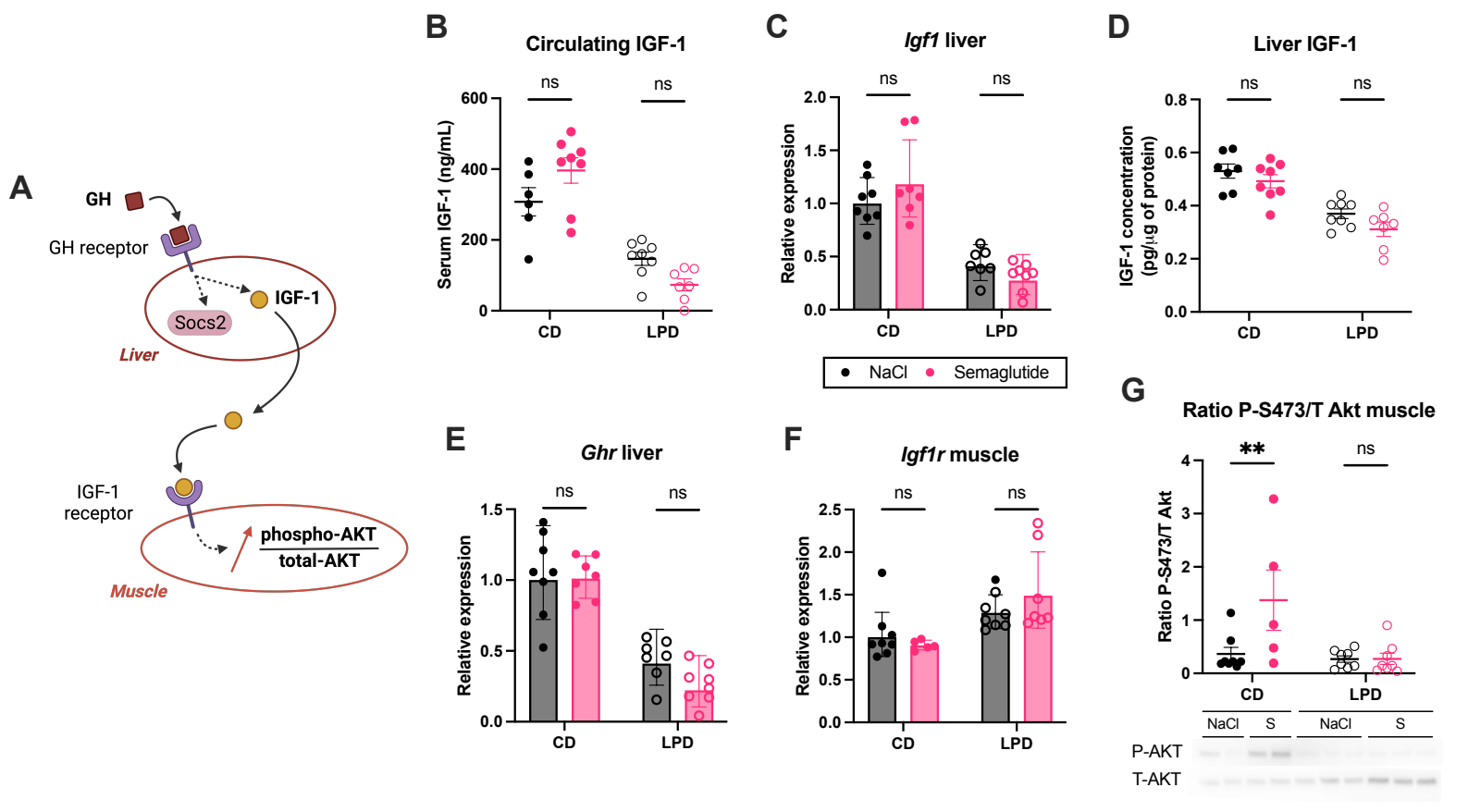
A
GH
GH receptor
IGF-1
Socs2
Liver
IGF-1
receptor
phospho-AKT
total-AKT
Muscle
B
Circulating IGF-1
Serum IGF-1 (ng/mL)
600
400
200
0
ns
ns
CD
LPD
C
Igf1 liver
Relative expression
2.0
1.5
1.0
0.5
0.0
ns
ns
CD
LPD
NaCl
Semaglutide
D
Liver IGF-1
IGF-1 concentration
(pg/µg of protein)
0.8
0.6
0.4
0.2
0.0
ns
ns
CD
LPD
E
Ghr liver
Relative expression
1.5
1.0
0.5
0.0
ns
ns
CD
LPD
F
Igf1r muscle
Relative expression
2.5
2.0
1.5
1.0
0.5
0.0
ns
ns
CD
LPD
G
Ratio P-S473/T Akt muscle
Ratio P-S473/T Akt
4
3
2
1
0
**
ns
CD
LPD
NaCl
S
NaCl
S
P-AKT
T-AKT

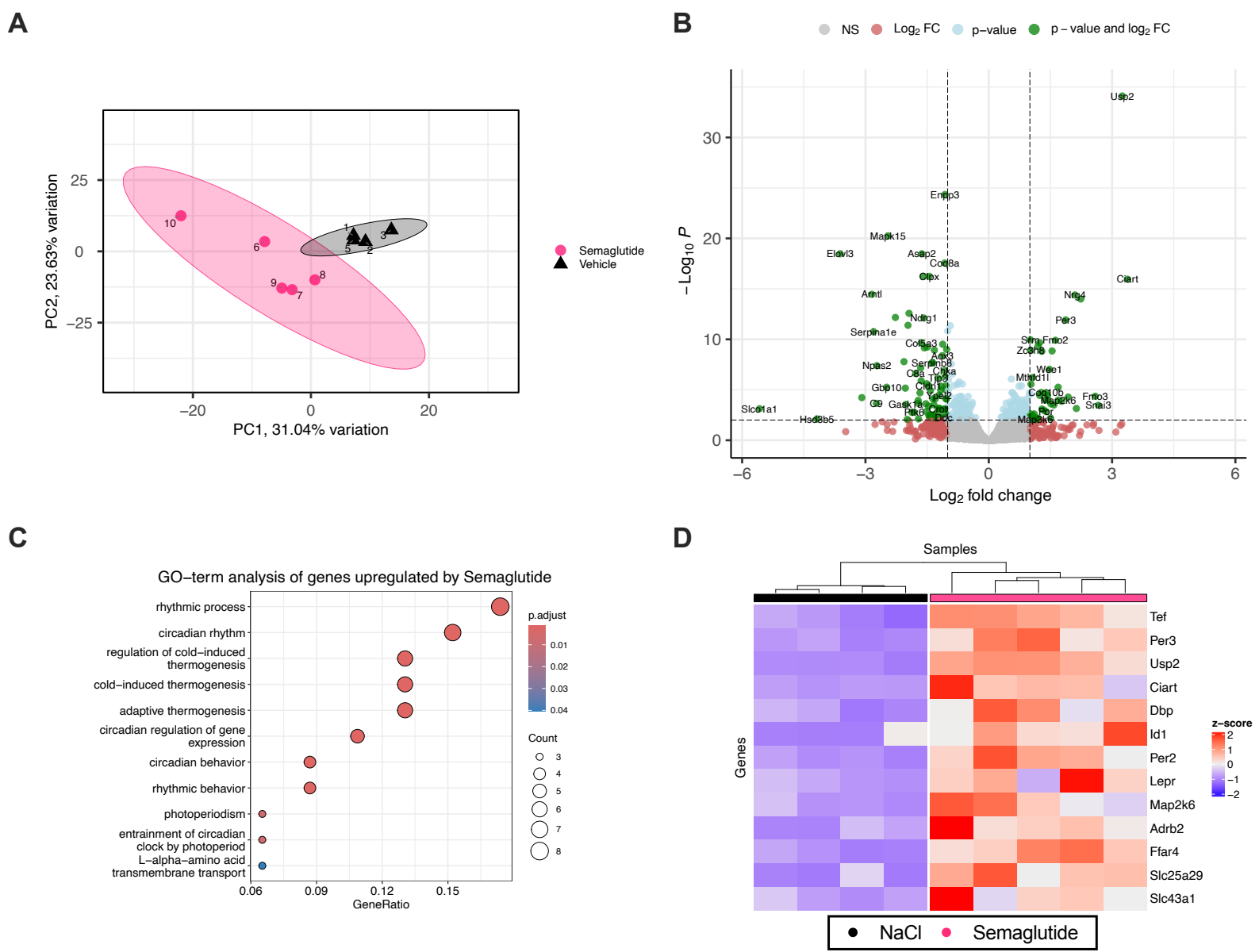
A
PC2, 23.63% variation
PC1, 31.04% variation
Semaglutide
Vehicle
B
NS
Log2 FC
p−value
p − value and log2 FC
−Log10 P
Log2 fold change
C
GO−term analysis of genes upregulated by Semaglutide
rhythmic process
circadian rhythm
regulation of cold−induced thermogenesis
cold−induced thermogenesis
adaptive thermogenesis
circadian regulation of gene expression
circadian behavior
rhythmic behavior
photoperiodism
entrainment of circadian clock by photoperiod
L−alpha−amino acid transmembrane transport
GeneRatio
p.adjust
Count
D
Samples
Genes
Tef
Per3
Usp2
Ciart
Dbp
Id1
Per2
Lepr
Map2k6
Adrb2
Ffar4
Slc25a29
Slc43a1
z−score
NaCl
Semaglutide